ELSEVIER

International Journal of Mass Spectrometry 182/183 (1999) 85–97

International Journal of Mass Spectrometry

Oxidation properties of the early transition-metal dioxide cations MO_2^+ (M = Ti, V, Zr, Nb) in the gas-phase

Jeremy N. Harvey[a], Martin Diefenbach[b], Detlef Schröder[b], Helmut Schwarz[b,*]

[a]*The Fritz-Haber Center for Molecular Dynamics, The Hebrew University, Jerusalem 91904, Israel*
[b]*Institut für Organische Chemie der Technischen Universität Berlin, Straße des 17. Juni 135, D-10623 Berlin, Germany*

Received 28 July 1998; accepted 10 September 1998

Abstract

Fourier-transform mass spectrometry is used to characterize the gas-phase reactivities of metal dioxide cations MO_2^+ (M = Ti, V, Zr, Nb) towards simple hydrocarbons. Thus, H-atom abstraction from water and methane by TiO_2^+ and ZrO_2^+ demonstrate the radical-type reactivity of these species. In marked contrast, VO_2^+ and NbO_2^+ behave as closed-shell species in that no radical losses occur. These reactivity patterns are in accord with a description of the bonding schemes of the metal dioxides. B3LYP calculations predict singlet ground states for VO_2^+ and NbO_2^+ and doublet ground states for TiO_2^+ and ZrO_2^+; the latter can be described as oxygen-centered radicals. In addition, the oxidations of ethene and ethane by vanadyl cation VO_2^+ are studied by ab initio theory. The oxidation of ethene by VO_2^+ is suggested to proceed via a conceptually new mechanism which involves a direct oxygen transfer from the metal to the olefin to afford acetaldehyde complexed to VO^+ as reaction product. (Int J Mass Spectrom 182/183 (1999) 85–97) © 1999 Elsevier Science B.V.

Keywords: Ab initio theory; Mass spectrometry; Metal dioxides; Oxidation; Vanadium oxides

1. Introduction

Transition metals are involved in many catalytic processes in nature and in large-scale industrial processes. Their ubiquitous presence is due to the ability of transition metals to adopt different oxidation states, coordination modes, bonding patterns, etc. This enormous diversity represents a challenge to chemists in their attempt to identify, understand, and then predict reaction mechanisms. One approach that has been quite fruitful in the last few years has been to study the reactions of bare metal ions in the gas phase [1]. In the absence of solvent and aggregation effects, the intrinsic reactivity of the metal can thus be understood to a much finer degree of detail than, for example, the action of bulk heterogeneous catalyst. However, atomic metal ions are of course rather simplified models of condensed-phase species, so there is an increasing trend to study the gas-phase properties of ligated transition-metal ions.

Ben S. Freiser was one of the pioneers in this area and was the first to perform numerous studies about the effects of ligands on the gas-phase reactivity of transition metal ions [2]. For example, Freiser's group systematically extended preliminary studies of Kappes and Staley [3] on the reactivity of FeO^+ cation with hydrocarbons [4], and so founded the branch of metal-catalyzed gas-phase oxidations also including effective mimics of catalytic cycles [3,5].

* Corresponding author.
In memory of Ben S. Freiser, a great friend and a fine scientist.

PII S1387-3806(98)14241-0

Meanwhile, the fascinating chemistry of transition-metal oxides has been examined by other groups as well [6]. Recently, also the gas-phase reactivities of some metal dioxide cations received increasing attention, e.g. CrO_2^+ [7], FeO_2^+ [8], NbO_2^+ [9,10], MoO_2^+ [11–13], CeO_2^+ [14], TaO_2^+ [9,10,15], OsO_2^+ [16], and ThO_2^+ [17]. Of prime interest in this context are oxidation reactions initiated by metal-dioxo species, processes that are widely applied and technologically relevant, e.g. the dihydroxylation of olefins. Here, we report the reactivities of the early transition-metal dioxide cations MO_2^+ (M = Ti, V, Zr, Nb) with some selected, small hydrocarbons. In addition to the experimental studies, the metal-dioxide cations and the potential-energy surfaces relevant to the reactivity of the vanadyl cation VO_2^+ are investigated by ab initio studies with density functional theory (DFT) methods.

2. Experimental and computational methods

The experiments were carried out using a *Spectrospin CMS 47X* FTICR mass spectrometer, which has been described in detail elsewhere [18]. In brief, the transition-metal cations M^+ (M = Ti, V, Zr, Nb) were generated in an external source by laser desorption/ionization [19] of the corresponding metal targets. By a system of electric potentials and lenses the cations were transferred to the analyzer cell, which is located within a superconducting magnet (maximum field strength 7.05 Tesla). The isolation of the metals' most abundant isotope and all subsequent mass-selections were performed using the FERETS technique [20], a computer controlled ion-ejection protocol that combines single-frequency pulses with frequency sweeps to optimize ion isolation. Generation of the metal-dioxide cations was performed by pulsing-in of a mixture of O_2 and N_2O (see below). In this procedure, the ions undergo several hundreds of collisions such that the product ions were assumed to be thermalized [21]. The mass-selected ions of interest were then reacted with neutral hydrocarbons, which were introduced to the FTICR cell via leak valves at stationary pressures in the order of 10^{-8} mbar. In the case of the group 4 dioxo-cations MO_2^+ (M = Ti, Zr), rapid reactions with background water to form MO_2H^+ were observed. In order to derive rate constants for the slower reactions with methane (see below), the rates of disappearance of MO_2^+ and of formation of MO_2H^+ were monitored at several pressures of CH_4. The slopes of the apparent unimolecular rate constants as a function of methane pressure were converted to the respective bimolecular rate constants [12,14]. To ascertain that the variations of the unimolecular constants were not due to mere pressure effects, the background reactions with water were also monitored in the presence of leaked-in argon gas, but no significant differences were found compared with the absence of argon. Rate constants were derived from the pseudo-first order rates in conjunction with the measured partial pressures of the neutral reactant gases. The error of the absolute rates amounts to ±30% and increases to ±50% when background correction is necessary. All data were accumulated and on-line processed using an ASPECT 3000 minicomputer.

In the computational studies the geometries of all calculated species were optimized at the B3LYP level of theory using basis sets of approximately double-zeta quality. For H, C, O, Ti, and V, these were the all electron split-valence basis sets of Schäfer, Horn, and Ahlrichs [22]. For Zr and Nb, the Hay-Wadt relativistic effective core potentials (RECP) were used to treat the $[Ar]3d^{10}$ core in conjunction with the associated LANL2DZ valence basis sets [23,24]; this combination is referred to as BS1. All stationary points were fully optimized at the B3LYP/BS1 level of theory, and their nature then determined by calculation of the force constants using the same method and basis set, with minima having only positive eigenvalues and transition structures having a single negative one [25]. The resulting vibrational frequencies were also used to correct for zero-point vibrational energy (ZPVE). At the geometries thus obtained, single-point energies were calculated using the larger BS2. For H, C, O, Ti, and V, again the standard all-electron 6-311 + G(2*d*,*p*) basis sets implemented in GAUSSIAN94 [26] were employed. For the metals, the Wachters-Hay all electron basis sets were combined with the scaling factors of Raghavachari and Trucks [27]. For Zr and Nb, the same RECPs [28]

Table 1
Selected thermochemical data[a] for MO and MO_2 species (M = Ti, V, Zr, Nb)

	D(M–O)[b]	IE(M–O)	$D(M^+–O)$	D(OM–O)	$IE(MO_2)$	$D(OM^+–O)$
Ti	159.6 ± 2.2	6.819 ± 0.006[c,d]	159.8 ± 2.1[f]	143.6 ± 2.3[d]	9.54 ± 0.1[d,i]	80.8 ± 2.3[k]
V	148.4 ± 4.5	7.2386 ± 0.0006[c,d]	138.1 ± 2.1[g]	131.9 ± 4.8[h]	10.5 ± 0.3[h,i,j]	70.6 ± 9.2[g]
Zr	184.4 ± 3.2	6.87 ± 0.18[e]	178.9 ± 2.5[e]	141.6 ± 6.9[d]	9.4 ± 0.2[d,i]	89.0 ± 1.6[k]
Nb	182.9 ± 5.0	7.91 ± 0.02[c,d]	164.4 ± 2.5[e]	154.0 ± 5.0[d]	8.94 ± 0.19[k]	131.7 ± 3.9[l]

[a]Ionization energies (IE) in eV, binding energies (*D*) in kcal/mol.
[b][30].
[c]IEs determined with photoelectron spectroscopy.
[d]Data extracted from the NIST chemistry webwook, see: http://webbook.nist.gov/chemistry.
[e][34].
[f][31].
[g][37].
[h][35].
[i]IEs determined as electron ionization threshold.
[j]This work suggests $IE(VO_2)$ = 9.5 ± 0.4 eV, see text.
[k][36].

as in BS1 were used and enlarged by one additional *s*, *p*, and *d* function, respectively, whose exponents were chosen to be 1/3 the size of the most diffuse function of each type already present in the basis, further complemented by an additional *f* function (α = 0.5 and 0.77 for Zr and Nb, respectively). All calculations were carried out using GAUSSIAN94 [26], and the energies given below refer to B3LYP/BS2//B3LYP/BS1 results including ZPVE.

3. Results and discussion

3.1. Ion formation, structure, and thermochemistry

The reactant ions for the present study were generated by reacting a pulsed-in mixture of O_2 and N_2O with the relevant bare metal ions M^+. The formation of the monoxo-cation MO^+, presumably following reaction (1), is already known to be fast, while reaction (2) to form MO_2^+ is much slower [3,9,10]. For example, the rate constant of 0.7×10^{-12} cm^3 $molecule^{-1}$ s^{-1} for reaction (2) with M = V, corresponds to a collision efficiency ϕ of only 0.0008; here, ϕ stands for the ratio of the bimolecular rate constant *k* and the gas-kinetic collision rate constant k_C. Notwithstanding, the yields of the MO_2^+ ions are in all cases acceptable because the ions undergo multiple collisions with the oxidants during the pulse sequence and do not undergo rapid consecutive reactions with either O_2 or N_2O.

$$M^+ + O_2 \rightarrow MO^+ + O \quad (1)$$

$$MO^+ + N_2O \rightarrow MO_2^+ + N_2 \quad (2)$$

In general, two types of bonding are conceivable for $[M,O_2]^+$ species [7,8,29]: one type that can be described as metal dioxide, i.e. $O–M^+–O$, and another to be regarded as metal-dioxygen complex $M^+–(O_2)$. The dioxide structure will be favored by those metals that form strong M–O bonds, while the second type becomes more relevant for those metals that have weaker M–O bonds and disfavor high oxidation states. Because of the strong M–O and OM–O bonds that are formed for early transition metals Ti, V, Zr, and Nb, the dioxide structures are expected to be clearly favored over those of the corresponding dioxygen complexes. This conjecture is in accord with the sequential mode of formation of the dioxo-cations via reactions (1) and (2), the available thermochemical information (Table 1), as well as the experimental finding that no exchange reactions occur in which a ligand replaces O_2. Finally, the inserted dioxide structures and their expected electronic structures correlate nicely with the observed reactivities (see below).

Fortunately, quite a number of bond dissociation energies (D) and ionization energies (IE) are available for the metal monoxide and dioxide cations under study (Table 1). Most of the values for the monoxides agree favorably well. For example, independently measured values D(Ti–O) = 159.6 ± 2.2 kcal/mol [30] and $D(Ti^+–O)$ = 159.7 ± 2.1 kcal/mol [31] together with IE(Ti) = 6.8282 eV [32] and IE(TiO) = 6.819 ± 0.006 eV [33] combine to an internally consistent thermochemical cycle with a fortuitous error of only 0.1 kcal/mol. However, some deviations occur even for the monoxides, and the most pronounced one seems to be associated with ZrO, for which three values of IE(ZrO) ranging from 5.8–6.4 eV have been measured, while IE(ZrO) = 6.87 ± 0.18 has been evaluated from the thermochemical cycle; for a discussion see [34]. Due to increasing experimental difficulties as well as propagation of errors, the situation becomes worse for the metal dioxides; nevertheless, the error bars are still quite acceptable. The maximum internal error occurs for vanadyl species VO_2 and VO_2^+, for which the thermochemical cycle has a mismatch of about 14 kcal/mol, which has cast some doubt on the accuracy of IE (VO_2) [37]. In fact, when thermalized VO_2^+ is reacted with hexafluorobenzene (IE = 9.9 eV), charge transfer is hardly observed, and the adduct $(C_6F_6)VO_2^+$ is formed instead. Furthermore, electron transfer to VO_2^+ is quite efficient from fluorobenzene (IE = 9.1 eV) and 1,2,4-trifluorobenzene (IE = 9.3 eV), and occurs at about half collision rate with iodomethane (IE = 9.5 eV). Given the reasonable assumption that charge transfer is not hindered by kinetic barriers, IE(VO_2) is thus bracketed as 9.5 ± 0.4 eV, thus yielding $D(OV^+–O)$ = 79.7 ± 10.3 kcal/mol.

In any case, it is obvious from the data that all four metal-dioxo cations discussed here have fairly large bond energies $D(OM^+–O)$, e.g. well above $D(N_2–O)$ = 38.6 kcal/mol. As a consequence of the high oxidation states [38], all four metal dioxides also have fairly high ionization energies (Table 1). Hence, the MO_2^+ cations might be expected to undergo charge-transfer processes with more polarizable reagents than the set of small hydrocarbons under examination [12,16]. Another general trend is that the metals of the second transition-metal row form stronger M–O bonds than those of the first row which coincides with the preference for higher oxidation states with 4d and 5d transition metals.

3.2. Reactivity studies

The scope of the present study is to seek patterns in the reactivity of the MO_2^+ species for M = Ti, V, Zr, and Nb, rather than to provide a comprehensive description of the whole manifold of reactions that may occur with saturated and unsaturated hydrocarbons. Thus, the selection of substrates is deliberately limited and our choice was oriented at the criterion to match fundamentally different types of reactivities, i.e. which is the first hydrocarbon, starting with methane, for which any bond activation occurs and what kind of processes take place.

In line with previous results, e.g. as far as methane activation is concerned, most metal dioxide cations studied here are found to be more reactive than the corresponding cationic bare metals and monoxides [4,6]. The dioxides MO_2^+ (M = Ti, V, Zr, Nb) also fall into two groups of markedly different reactivity, which nicely correlate with the valence configurations of the metal atoms.

Therefore, let us briefly address the conceptual bonding schemes of the metal dioxides. Titanium and zirconium have four valence electrons as neutral atoms. In the neutral dioxides, these group 4 metals are thus able to form two strong double bonds with the oxygen atoms leading to singlet ground states. As with other high-valent metal oxides that have a closed-shell structure, e.g. MoO_3 and OsO_4 [12,16], the resulting TiO_2 and ZrO_2 neutrals are expected to have rather high ionization energies, since upon ionization an electron must be removed either from an M–O bonding π orbital or from a lone pair on oxygen (Scheme 1). Accordingly, one would expect TiO_2^+ and ZrO_2^+ to behave as reactive open-shell species in terms of abstraction processes typical for oxygen-centered radicals.

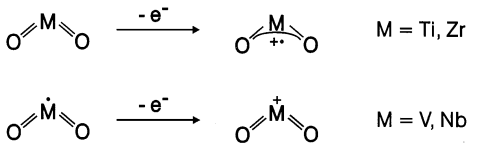

Scheme 1.

$$TiO_2^+ + H_2O \rightarrow TiO_2H^+ + HO^{\cdot} \qquad \phi \approx 1.0 \qquad (3)$$

$$ZrO_2^+ + H_2O \rightarrow ZrO_2H^+ + HO^{\cdot} \qquad \phi \approx 1.0 \qquad (4)$$

$$TiO_2^+ + CH_4 \rightarrow TiO_2H^+ + CH_3^{\cdot} \qquad \phi = 0.072 \qquad (5)$$

$$ZrO_2^+ + CH_4 \rightarrow ZrO_2H^+ + CH_3^{\cdot} \qquad \phi = 0.036 \qquad (6)$$

In fact, both ions react rapidly with background water and somewhat more slowly with methane to generate the formally closed-shell species MO_2H^+ (reactions 3–6). The rates of reactions (3) and (4) have not been measured explicitly, but due to the fact that both processes proceed rapidly already with the background ($p < 2 \times 10^{-9}$ mbar), we assume that these occur near collision rate. Reactions (5) and (6) are more than an order of magnitude slower. Moreover, the ionic products can of course not be distinguished from those of reactions (3) and (4). Therefore, the apparent unimolecular rate constants (k_{app}) for the disappearance of the reactant ions have been measured at different pressures of methane. Using $k_{app} = [k_{(3,4)} \cdot p_{H_2O} + k_{(5,6)} \cdot p_{CH_4}]$, the values $k_{(5)} = 0.74 \times 10^{-10}$ cm^3 molecule^{-1} s^{-1} and $k_{(6)} = 0.37 \times 10^{-10}$ cm^3 molecule^{-1} s^{-1} can be derived from the slopes of the k_{app}/p_{CH_4} graphs. In addition, reaction (5a) of TiO_2^+ with CD_4 was studied in the same way, yielding $k_{(5a)} = 0.45 \times 10^{-10}$ cm^3 molecule^{-1} s^{-1}. Although the initial product of this reaction should be TiO_2D^+, the main product observed experimentally was TiO_2H^+ due to the rapid, presumably collisional H/D exchange reaction (7) with background water.

$$TiO_2^+ + CD_4 \rightarrow TiO_2D^+ + CD_3^{\cdot} \qquad \phi = 0.048 \qquad (5a)$$

$$TiO_2D^+ + H_2O \rightarrow TiO_2H^+ + HDO \qquad (7)$$

Upon continuously ejecting the TiO_2D^+ during reaction of TiO_2^+ with CD_4 in a double-resonance experiment, the rate of formation of TiO_2H^+ strongly decreases, thus demonstrating that part of this product is indeed formed by the consecutive occurrence of reactions (5a) and (7). The ratio $\phi_{(5)}/\phi_{(5a)} = 1.5 \pm 0.2$ implies a moderate size of the intermolecular kinetic isotope effect for the activation of CH_4 and CD_4, respectively. This magnitude of the isotope effect is typical for an exothermic, radical-type H/D atom abstraction; for example, the activation of methane over Li/MgO catalysts—which is known to proceed via surface-bound oxygen radical sites—is associated with $k_{CH_4}/k_{CD_4} = 1.3$–1.6 [39,40].

The rapid occurrence of reactions (3) and (4) provides a lower limit for $D(OMO^+–H) > 119$ kcal/mol (M = Ti, Zr) and also suggests relatively high proton affinities (PA) of the metal dioxides, i.e. $PA(TiO_2) > 213$ kcal/mol and $PA(ZrO_2) > 216$ kcal/mol. The high bond energies can be understood, if one appreciates that the MO_2H^+ ions are essentially protonated MO_2 species, and thus benefit from the strong M–O bonding present in the neutral dioxides, unlike their open-shell MO_2^+ congeners. The mere occurrence of H atom abstraction from water implies that C–H bond activation of methane by TiO_2^+ and ZrO_2^+ is exothermic by at least 15 kcal/mol. Nevertheless, reactions (5) and (6) are relatively inefficient, which can be attributed to the low polarizability of methane such that the encounter complexes $[MO_2^+ \cdot CH_4]$ are short-lived. On the contrary, the complexes formed with water are expected to reside in significantly deeper wells due to the large dipole moment of water and the highly polarized metal core in MO_2^+. This result highlights the decisive role of reaction kinetics over and beyond any thermochemical considerations. Similar results have been observed with other open-shell metal oxide cations, such as ThO_2^+, which abstracts a hydrogen atom from water in analogy to reactions (3) and (4) but does not react at an observable rate with methane [17].

The group 5 dioxide cations display quite a different reactivity pattern, which can also be traced back to their bonding scheme. Thus, V and Nb neutral atoms have five valence electrons and form dioxides having

two strong M–O double bonds, leaving one unpaired electron on the metal. The corresponding cations arise from ionization of the metal cores and are thus closed-shell species (Scheme 1). Accordingly, the group 5 dioxides MO_2^+ (M = V, Zr; for Ta, see [10,15]) should not display the radical-type reactivity of their group 4 congeners. This conjecture is indeed found to hold true in that no atom abstractions are observed for VO_2^+ and ZrO_2^+ with the chosen substrates; for example, both ions are inert toward water and methane. However, the progressive contraction of the *d* orbitals along the transition-metal row in conjunction with the high partial positive charge on the metal induced by the two oxo ligands decreases the M–O bond strengths in MO_2^+ as compared with the neutral counterparts (Table 1). This feature may explain how the closed-shell species VO_2^+ and NbO_2^+ are capable of activating some larger alkanes and alkenes (reactions 8–10).

$$VO_2^+ + C_2H_6 \rightarrow [V,H_2,O_2]^+ + C_2H_4 \qquad \phi = 0.12 \tag{8}$$

$$VO_2^+ + C_2H_4 \rightarrow VO^+ + CH_3CHO \quad 90\% \qquad \phi = 0.45 \tag{9a}$$

$$\rightarrow [V,H_2,O_2]^+ + C_2H_2 \quad 10\% \tag{9b}$$

$$NbO_2^+ + C_3H_8 \rightarrow [Nb,C_3,H_6,O_2]^+ + H_2 \qquad \phi = 0.20 \tag{10}$$

Activation of ethane in reaction (8) leads to $[V,H_2, O_2]^+$ which could be either the dihydroxyvanadium cation $V(OH)_2^+$ or the water complex of vanadium monoxide cation, $(H_2O)VO^+$; thermochemistry implies that ethene is the neutral product. A similar pathway is observed in the reaction of VO_2^+ with ethene leading to neutral ethyne and $[V,H_2,O_2]^+$. Reaction (9b) is a minor channel, however, while VO^+ is the main product (reaction 9a), presumably involving acetaldehyde rather than ethylene oxide as the neutral product (see below). In line with the better donor properties of ethene, the reaction efficiency increases significantly from ethane to ethene.

Niobium dioxide cation is unreactive toward ethane and ethene. Hence, propane was chosen as a more reactive substrate, which is indeed activated by NbO_2^+ though with moderate efficiency. In marked contrast to the other dioxides, however, dehydrogenation rather than H-atom abstraction or oxygen-atom transfer is observed. The structure of the ionic product formed in reaction (10) can be deduced from its consecutive reaction with background water in which C_3H_6 is replaced by water to yield $[Nb,H_2,O_3]^+$. Hence, the ionic product formed in reaction (10) is assigned as a complex between propene and NbO_2^+, i.e. $(C_3H_6)NbO_2^+$. We note in passing that the $[Nb,H_2,O_3]^+$ ion associates rapidly with another water molecule to afford $[Nb,H_4,O_4]^+$, while no higher water adducts are observed at longer reaction times. This finding indicates a particular stability of this product ion, which might either be a $NbO_2(H_2O)_2^+$ complex or niobium tetrahydroxide, $Nb(OH)_4^+$. The latter ion is also formed as a terminal product in the ion chemistry of niobium in flames [41].

In general, the reaction patterns can be classified in terms of the occurrence of redox processes initiated by the metal dioxide cations. Thus, H-atom abstraction by MO_2^+ (M = Ti, Zr) can be described as a reduction of the metal dioxide cation radicals leading to the ionized metal oxo hydroxides $OMOH^+$. Whereas in the case of Ti and Zr the oxidation state of the *metal center* remains unchanged, the reactions of VO_2^+ can be described in terms of a reduction from V(V) to V(III) concomitant with oxidation of the organic substrate. In contrast, the dehydrogenation observed for the NbO_2^+/propene couple does not involve the oxoligands, which can rather be considered to act as mere spectators [42]. Hence, the oxidation state Nb(V) is maintained during C–H bond activation of propane suggesting σ-bond metathesis as the mechanism for dehydrogenation of propane [10]. Qualitatively, these reaction patterns can be under-

stood by (i) the large H-atom affinities of the radical-type species TiO_2^+ and ZrO_2^+ and (ii) the different OM^+–O bond strengths in for M = V and Nb. Thus, in the transition $VO_2^+ \rightarrow [V,H_2,O_2]^+$ one or both of the V–O bonds needs to be broken while two strong O–H bonds are formed. On the other hand, the Nb–O bonds in the $(C_3H_6)NbO_2^+$ products are not expected to dramatically differ from those in free NbO_2^+. Due to the fact that the M–O bonds are much stronger with niobium, the preference for simple dehydrogenation also finds a rationale. Nevertheless, formal oxygenation by NbO_2^+ is possible provided that the reactivity of the substrate is further enhanced. For example, NbO_2^+ reacts with butadiene to afford inter alia the interesting $[Nb,C_4,H_4,O]^+$ cation [9] concomitant with neutral water (15%), thus demonstrating the rupture of at least one Nb–O bond; other products are $[Nb,C_4,H_4,O_2]^+ + H_2$ (65%), $[Nb,C_2,H_4,O_2]^+ + C_2H_2$ (15%), and $[Nb,C_2,H_2,O_2]^+ + C_2H_4$ (5%).

3.3. Computational studies

In order to correlate the chemical behavior of the metal dioxide ions with their intrinsic molecular properties, complementary theoretical study of the neutral and cationic metal mono- and dioxides is indicated. In addition, the particularly interesting chemistry of the vanadyl ion VO_2^+ with ethane and ethene seems to be worth a theoretical consideration.

For the rather broad range of calculations that need to be carried out, several ab initio theoretical methods can be considered, but the peculiar nature of the bonding in these transition metal systems places severe restrictions on the applicability of most methods. Thus, it is well-known that bonding in transition metal oxides, especially those of the first row (Sc − Cu), is subject to very strong near-degeneracy and correlation effects, which put rather high demands to the methods employed. Let us illustrate this statement by the fact that the bond energy $D(OV^+–O)$ is *negative* by as much as −66 kcal/mol at the self-consistent field Hartree-Fock level with BS2. Upon incorporating the Møller-Plesset perturbational correction at second order (MP2), which is known to exaggerate correlation effects in cases when the HF reference wavefunction does not represent the bonding adequately, $D(OV^+–O)$ is mismatched in the other extreme and becomes 201 kcal/mol. These two values are respectively well below and above the experimental value of 70.6 ± 9.2 kcal/mol [37] and our best theoretical estimate of 90 kcal/mol (see below). Multireference methods hence appear very much indicated, but these require rather large basis sets and are computationally very demanding in themselves.

Density functional theory, on the other hand, is an economical approach that can in principle yield exact results at an expense that is barely higher than that of Hartree–Fock calculations. In particular, the B3LYP hybrid density functional has been shown to produce excellent thermochemistry for the compounds of the G2 set [43] and also provides a reasonable treatment for many systems involving first-row transition metals. Although the accuracy of density functional methods for describing transition states is somewhat limited, the results should be more than adequate for the semiquantitative aim of the present study. Moreover, with DFT even moderate-sized basis sets provide adequate geometries, and all optimizations in this study were performed with a small, split-valence basis set (BS1) of roughly double-zeta quality [22]. Although DFT in general requires smaller basis sets than standard correlation methods, a minimal requirement for obtaining reliable energetics in the present systems also involving ion-molecule complexes, are basis sets with diffuse functions on the heavy atoms and polarization functions on all atoms. Thus, the energetics were evaluated by B3LYP single point calculations at the B3LYP/BS1 geometries but with the much larger 6-311 + $G(2d,p)$ basis set (BS2). In general, most of the relative energies obtained with either basis set were fairly similar, except for dissociation energies, which were generally larger with BS2.

The calculated properties of the metal dioxides (Table 2) agree well with the bonding pattern outlined above (Scheme 1); there is not much to discuss about the monoxides [6,44,45]. The group 4 dioxide cations TiO_2^+ and ZrO_2^+ are predicted to have doublet ground states and population analysis reveals significant spin density on oxygen. Instead, the group 5 dioxide

Table 2
Electronic ground states,[a] geometries, and vibrational frequencies[b] of neutral and cationic MO and MO_2 species (M = Ti, V, Zr, Nb) calculated with B3LYP/BS1[c]

	State	r_{M-O}	α_{OMO}	$\omega_{sym.stretch}$ (A_1)	$\omega_{asym.stretch}$ (B_2)	$\omega_{bending}$ (A_1)
TiO	$^3\Delta$	1.621		1044.3		
TiO^+	$^2\Delta$	1.586		1109.5		
TiO_2	$^1A_1$	1.644	111.3	1037.5	1024.4	378.7
TiO_2^+	$^2B_2$	1.664	95.1	967.6	217.3	261.6
VO	$^4\Sigma^-$	1.595		1025.8		
VO^+	$^3\Sigma^-$	1.556		1102.2		
VO_2	$^2A_1$	1.612	112.6	1043.1	1042.7	358.4
VO_2^+	$^1A_1$	1.564	106.4	1125.2	1111.4	458.2
ZrO	$^3\Delta$	1.775		960.4		
ZrO^+	$^2\Delta$	1.743		1001.0		
ZrO_2	$^1A_1$	1.806	107.4	932.5	895.0	298.8
ZrO_2^+	$^2B_2$	1.828	95.2	882.9	90.8	190.5
NbO	$^4\Sigma^-$	1.726		1002.7		
NbO^+	$^3\Sigma^-$	1.696		1045.1		
NbO_2	$^2A_1$	1.750	105.0	987.5	953.2	333.7
NbO_2^+	$^1A_1$	1.717	102.8	1034.0	998.8	380.2

[a]The ground state assignments refer to the B3LYP/BS2//B3LYP/BS1 energies.
[b]Unscaled frequencies.
[c]Bond lengths in Ångstroms, angles in degrees, and frequencies in cm^{-1}.

cations VO_2^+ and NbO_2^+ are singlets. Further, all metal dioxides studied here are bent due to favorable overlap of the metals' *d*-orbitals with the 2*p* orbitals of the oxygen atoms in a bent geometry; this phenomenon has been discussed by Siegbahn in a previous study of the neutral oxides of the 4*d* series [46]. Further, the agreement of the previous theoretical results for the 4*d* metals [45,46] and our data is satisfactory. With respect to the present reactivity studies, the different bonding situations of the group 4 versus group 5 dioxide cations is most interesting. In fact, the tentative bonding scheme is nicely corroborated by the theoretical results. For example, in all mono- and dioxides the M–O bond lengths decrease from the neutral to the cation except for the TiO_2/TiO_2^+ and ZrO_2/ZrO_2^+ couples. This bond elongation in TiO_2^+ and ZrO_2^+ can be regarded as a direct consequence of the loosening of these M–O bonds upon ionization to the cation radicals. In analogy, all MO_2 frequencies decrease in the cations for M = Ti and Zr while they increase for M = V and Nb. Finally, the particular bonding situation in TiO_2^+ and ZrO_2^+ is reflected by the almost perpendicular OMO arrangement while all other neutral and charged dioxides have bond angles of about 107 ± 5°.

Let us now address the thermochemical properties (Table 1) of the neutral and cationic metal oxides $MO_n^{o/+}$ (M = Ti, V, Zr, Nb; *n* = 1, 2) in order to evaluate the reliability of the computational approach (Table 3). Considering that the B3LYP approach is of

Table 3
Calculated (B3LYP/BSII//B3LYP/BSI + ZPVE) thermochemical data[a] for MO and MO_2 species (M = Ti, V, Zr, Nb)

	D(M–O)	IE(M–O)	$D(M^+–O)$	D(OM–O)	IE(MO_2)	$D(OM^+–O)$
Ti	158.9	7.04	154.1	136.7	9.62	77.1
V	150.9	7.50	128.3	123.5	8.95	90.2
Zr	174.8	6.90	165.9	141.8	9.03	92.5
Nb	170.1	7.35	159.5	144.4	8.13	126.5

[a]Chemical data correspond to 0 K values. Ionization energies (IE) in eV, dissociation energies (D) in kcal/mol.

limited accuracy for coordinatively unsaturated transition metal compounds, the comparison of the data collected in Tables 1 and 3 shows acceptable agreement. Thus, the largest deviations between experiment and theory occur for niobium in that theory underestimates all Nb–O binding energies by 5–13 kcal/mol.

One case deserves special notice, i.e. the vanadyl cation VO_2^+, whose reactions will be examined in some detail further below. Thus, another major deviation is the mismatch of the experimental and calculated IE(VO_2). As discussed above, the experimental value is likely to be too high, and the value of 9.5 ± 0.4 eV obtained in this work by charge-transfer bracketing agrees much better with the calculated figure (8.95 eV); the calculated figure is presumably slightly underestimated by a few tenths of an eV. The calculated bond energy $D(OV^+–O)$ is 90 kcal/mol, and judging from the other data, this value is if anything a few kcal/mol too low. Although the experimental value $D(OV^+–O) = 70.6 \pm 9.2$ kcal/mol [37] has been determined via threshold measurements which often yield very accurate results for transition metal species [47], the rather large discrepancy casts some doubt on the reliability of the experimental value. In particular, the experimental $D(OV^+–O)$ has been derived from the apparent threshold of the high energy reaction (11), which has to compete with a much more efficient channel to produce V^+ cation [37].

$$VO^+ + CO \rightarrow VO_2^+ + C \quad (11)$$

Considering this competition as well as the fact that the reaction will clearly involve a major electronic rearrangement—although it is formally spin-allowed, leading from VO^+ ($^3\Sigma^-$) and CO ($^1\Sigma^+$) to VO_2^+ ($^1A_1$) and C (^3P)—the formation of VO_2^+ is a very inefficient process. Thus, the experimental figure may only be regarded as a lower limit of $D(OV^+–O)$. We note in passing that in the same study no more than a lower limit of $D(OV^+–O) > 41.5 \pm 11.5$ kcal/mol could be determined in the reaction of V^+ with CO_2 to afford $VO_2^+ + C$ [37], thus clearly demonstrating the influence of kinetic parameters. We shall not dwell on the mere discussion of the accuracy of the thermochemical data, but our motivation to doubt the experimental figure is the *trend* among the metal dioxides. Thus, there exists no obvious reason why $D(OM^+–O)$ should be smaller and IE(MO_2) should be larger for the closed-shell species (M = V) as compared with its open-shell congeners (M = Ti, Zr), as implied by the experimental data. Instead, the computed trends of $D(OM^+–O)$ and IE(MO_2) appear much more intuitive in terms of the bonding pattern.

The second part of the computational study addresses the reactivity of vanadyl cation with ethane and ethene. These two particular reactions were chosen on the following grounds. At first, our prime interests are oxidation reactions and oxygen atom transfers; accordingly, the dehydrogenation of propane by NbO_2^+ with the oxygen atoms serving as mere spectator ligands is of lower priority. Next, the H-atom abstractions induced by TiO_2^+ and ZrO_2^+ are mechanistically less intriguing because such reactions can be assumed to be associated with low barriers typical for processes involving oxygen-centered radicals. Thus, for the reactions of TiO_2^+ and ZrO_2^+ the major features of the respective potential-energy surfaces are fixed by the mere thermodynamic properties of reactants and products. The reactions of VO_2^+, however, reveal two intriguing aspects in that (i) the oxidation state of the metal changes from V(V) to V(III) and (ii) this altered valence goes hand in hand with a change in the spin multiplicity because VO_2^+ is a singlet while the V(III) species have triplet ground states.

For the VO_2^+/ethane couple, $[V,O_2,H_2]^+$ is the only ionic product observed concomitant with neutral ethene (reaction 8). According to the B3LYP calculations (Fig. 1), the first step is the formation of the ion-molecule complex **1**, which appears to be mostly electrostatic in nature and involves essentially no perturbation of the substructures. Then, in the four-centered transition structure **TS1/2** there occurs a C–H bond insertion across the relatively weak V–O double bond. As expected, **TS1/2** displays elongated V–C, O–H, and C–H bonds as compared with reactants and products, respectively (Fig. 2). The computed activation barrier associated with this process

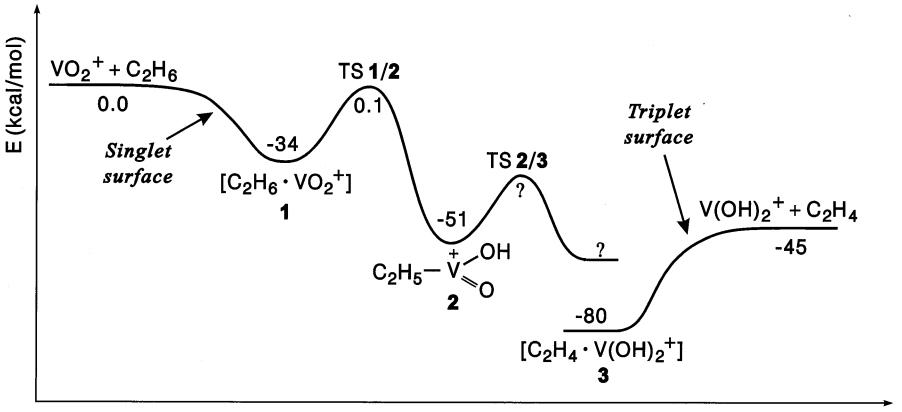

Fig. 1. Schematic potential-energy surface for the reaction of ethane with VO_2^+ according to B3LYP/BS2//B3LYP/BS1 calculations; energies relative to the entrance channel are given in kcal/mol. Note that the reactants are singlets while the products arise from the triplet surface.

sets an energy demand for bond activation that is right at the entrance level of the isolated reactants, thus providing a possible explanation for the moderate efficiency of reaction (8). The product **2** formed after passage via **TS1/2** may be described as an O-protonated ethyl vanadium dioxide, i.e. a new type of high-valent organometal oxide [48]. Formation of **2** is quite exothermic, and β-hydrogen transfer from the alkyl group to the oxo unit leads to **3**, which represents the direct precursor en route to product formation. Note that somewhere in between **2** and **3** the system must undergo a spin inversion because the formal V(V) compound **2** is a singlet, while the V(III) species **3** and $V(OH)_2^+$ have triplet ground states. Unlike other systems [49,50], however, we do not attribute a major mechanistic role to the spin crossover, because it occurs well after the presumably rate-determining C–H bond activation and involves species which are formed with large excess energies such that many rovibrational modes are excited and even electronically excited states may be accessible. Consequently, spin-inversion is not regarded as a rate-limiting factor but rather as a later step occurring in the exit channel.

The reaction of VO_2^+ with ethene is examined with the same theoretical approach (Fig. 3), but only reaction (9a) as the major channel leading to the formation of VO^+ along with neutral $[C_2,H_4,O]$ is considered. In this case, the structure of the reactant

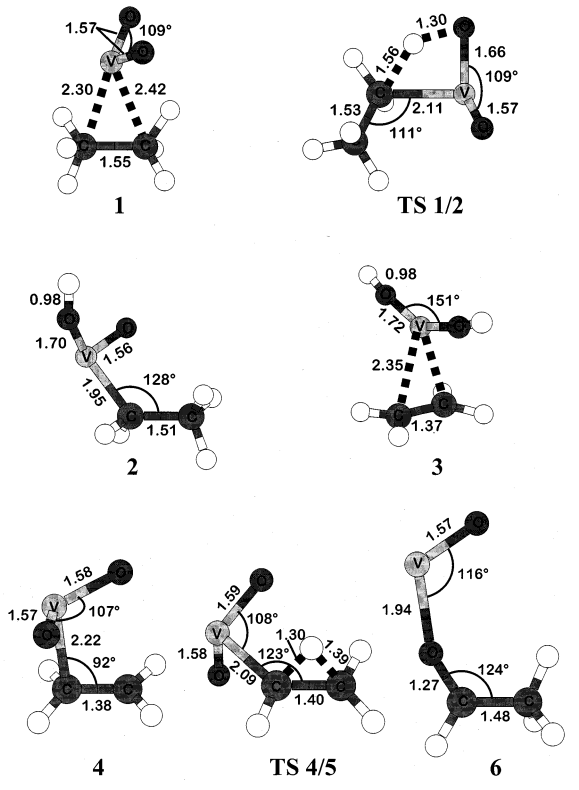

Fig. 2. Selected geometric parameters of the species involved in the reaction of VO_2^+ with ethane and ethene, respectively, calculated at the B3LYP level of theory using the split-valence basis set BS1; bond lengths in Å and angles in degrees. The singlet electromer of **6** is not shown, because only the V–C bond lengths differ significantly from the triplet (1.89 Å for the singlet versus 1.94 for the triplet).

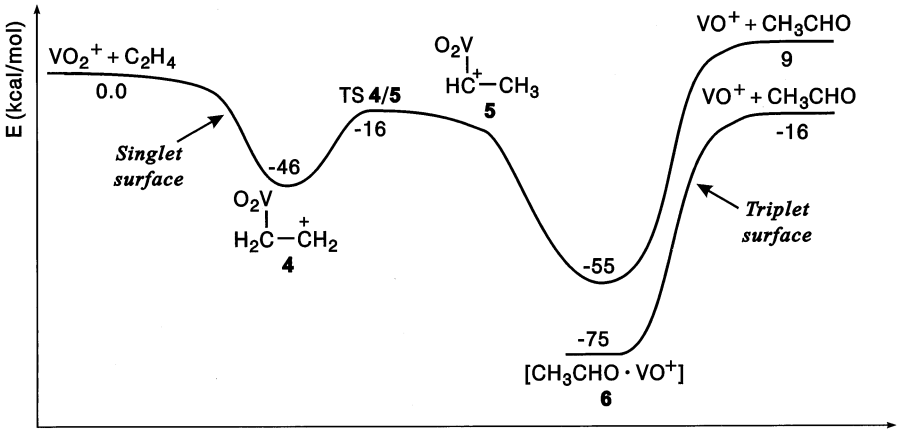

Fig. 3. Schematic potential-energy surface for the reaction of ethene with VO_2^+ according to B3LYP/BS2//B3LYP/BS1 calculations; energies relative to the entrance channel are given in kcal/mol. Note that the reactants are singlets while the lowest-lying product channel arises from the triplet surface.

complex **4** is worth a more detailed discussion (Fig. 2). Thus, unlike many other metal ethene complexes [51], the metal unit is *not* coordinated symmetrically to the methylene groups in **4**, but coordinated to one of the methylene groups in an almost perpendicular manner (α_{MCC} = 92°). Moreover, the V–C bond length of 2.22 Å indicates a covalent interaction between vanadium and carbon. Of course, V–C bond formation is associated with a significant elongation of the C–C bond to 1.38 Å. As a direct consequence of the singlet situation, the population analysis reveals that the positive charge is effectively located at the terminal methylene group. Accordingly, **4** can be compared to one of those intermediates that are formed upon the addition of hard electrophiles to olefins and correspond to carbocations instead of cyclic onium ions. The carbocationic character of **4** also accounts for the ~30 kcal/mol barrier associated with **TS4/5**, which can be regarded as a 1,2-hydride transfer between the adjacent carbon atoms. This rearrangement is a typical process occurring in carbocations, and here, it formally leads from the primary carbocation **4** to **5** as a substituted one. Structure **5** is, however, neither a minimum nor a TS, but only a transient along the intrinsic reaction coordinate leading to the formation of the product complex **6** via rotation of the vanadyl unit. Adopting the singlet surface of the reactants, ^{1}**6** shall be formed initially. The triplet state ^{3}**6** is, however, some 20 kcal/mol lower in energy, and the close geometries along with the excess energy with respect to the reactants shall render crossing from the singlet to the triplet surface quite efficient. Hence, B3LYP predicts the formation of VO^+ ($^3\Sigma^+$) ground state and acetaldehyde as reaction products. In fact, the calculation demands for this particular product channel, because spin-allowed formation of VO^+ ($^1\Delta$) + CH_3CHO as well as epoxidation, i.e. VO^+ ($^3\Sigma^+$) + *c*-C_2H_4O, are predicted to be endothermic with respect to the entrance channel. Further, we searched for other transition structures which would resemble oxidation of **4** via [2 + 2] or [3 + 2] cycloadditions of the vanadyl across the C–C bond leading to the corresponding metallaoxetanes and metal diolates, respectively. However, all structures found were well above the entrance channel of isolated VO_2^+ + C_2H_4, prompting us to exclude these pathways to occur at thermal energies.

The course of reaction (9a) via **TS4/5** and transient **5** to yield **6** has an important implication for the oxygenation to olefins. Thus, this sequence depicts a route for O-atom transfer to an olefin and rearrangement to the carbonyl compound in a *single* mechanistic step. Very often, however, it is indeed desired to *exclude* this particular route in metal-catalyzed oxygenation in favor of olefin epoxidation [6]. The mechanistic analysis clearly demonstrates that the

prime reason for the rearrangement **4** → **6** is the carbocationic nature of the intermediates. Thus, it is by and large the Lewis acidity of the vanadyl which prompts the isomerization into acetaldehyde, suggesting that this particular property should be minimized in developing effective epoxidation catalysts.

4. Conclusions

The reactivity patterns of the metal dioxide cations TiO_2^+, VO_2^+, ZrO_2^+, and NbO_2^+ can consistently be described in terms of their electronic and thermochemical properties. Thus, TiO_2^+ and ZrO_2^+ behave as oxygen-centered radicals capable of abstracting H atom from water and methane. The singlet species VO_2^+ and NbO_2^+ react markedly different. Thus, efficient O atom transfer to organic substrates is observed for VO_2^+, while the oxo ligands behave as mere spectators in NbO_2^+. Further, comparison of experiment and theory also demonstrates that density functional theory can be used to semiquantitatively assess the gas-phase energetics of neutral and charged transition-metal oxides and dioxides, a task which is far from being trivial due to the tremendous correlation effects in these species. Further, the calculated potential-energy surface for the oxygen transfer from VO_2^+ to ethene reveals a new direct route for the transformation $C_2H_4 + \langle O \rangle \rightarrow CH_3CHO$ via a coupled oxidation and hydrogen migration.

Note added in proof: A recent photoionization study [H.-P. Loock, B. Simard, S. Wallin, C. Linton, J. Chem. Phys. 109 (1998) 8980] reports IE(TiO) = 6.8197(7) eV, IE(ZrO) = 6.812(2) eV, and IE(NbO) = 7.154(1) eV. The data for TiO and ZrO are reasonably consistent with those in Tables 1 and 3, while IE(NbO) is much closer to the calculated value than the previous experimental figure.

Acknowledgments

Financial support by the Deutsche Forschungsgemeinschaft, the Fonds der Chemischen Industrie, the Volkswagen Stiftung, and the Gesellschaft von Freunden der Technischen Universität Berlin is acknowledged. M.R. Sievers and P.B. Armentrout are appreciated for communicating to us unpublished results from [36]. We also acknowledge the Konrad–Zuse–Zentrum for generous allocation of computer time.

References

[1] For an introduction, see B.S. Freiser, J. Mass Spectrom. 31 (1996) 703.
[2] S.W. Buckner, B.S. Freiser, Polyhedron 7 (1988) 1583.
[3] M.M. Kappes, R.H. Staley, J. Phys. Chem. 85 (1981) 942.
[4] T.C. Jackson, D.B. Jacobson, B.S. Freiser, J. Am. Chem. Soc. 106 (1984) 1252.
[5] S.W. Buckner, J.R. Gord, B.S. Freiser, J. Am. Chem. Soc. 110 (1988) 6606.
[6] D. Schröder, H. Schwarz, Angew. Chem., Int. Ed. Engl. 34 (1995) 1973.
[7] A. Fiedler, I. Kretzschmar, D. Schröder, H. Schwarz, J. Am. Chem. Soc. 118 (1996) 9941.
[8] D. Schröder, A. Fiedler, J. Schwarz, H. Schwarz, Inorg. Chem. 33 (1994) 5094.
[9] R.M. Pope, S.L. VanOrden, B.T. Cooper, S.W. Buckner, Organometallics 11 (1992) 2001.
[10] R.M. Pope, S.W. Buckner, Org. Mass Spectrom. 28 (1993) 1616.
[11] C.J. Cassady, S.W. McElvany, Organometallics 11 (1992) 2367.
[12] I. Kretzschmar, A. Fiedler, J.N. Harvey, D. Schröder, H. Schwarz, J. Phys. Chem. A 101 (1997) 6252.
[13] I. Kretzschmar, D. Schröder, H. Schwarz, Int. J. Mass Spectrom. Ion Processes 167/168 (1997) 103.
[14] C. Heinemann, H.H. Cornehl, D. Schröder, M. Dolg, H. Schwarz, Inorg. Chem. 35 (1996) 2463.
[15] R. Wesendrup, H. Schwarz, Angew. Chem. Int. Ed. Engl. 34 (1995) 2033.
[16] K.K. Irikura, J.L. Beauchamp, J. Am. Chem. Soc. 111 (1989) 75.
[17] H.H. Cornehl, R. Wesendrup, M. Diefenbach, H. Schwarz, Chem. Eur. J. 3 (1997) 1083.
[18] K. Eller, H. Schwarz, Int. J. Mass Spectrom. Ion Processes 93 (1989) 243.
[19] B.S. Freiser, Talanta 32 (1982) 697.
[20] R.A. Forbes, F.H. Laukien, J. Wronka, Int. J. Mass Spectrom. Ion Processes 83 (1988) 23.
[21] D. Schröder, H. Schwarz, D.E. Clemmer, Y. Chen, P.B. Armentrout, V.I. Baranov, D.K. Bohme, Int. J. Mass Spectrom. Ion Processes 161 (1997) 175.
[22] A. Schäfer, H. Horn, R. Ahlrichs, J. Chem. Phys. 97 (1992) 2571.
[23] A.J.H. Wachters, J. Chem. Phys. 52 (1970) 1033.
[24] P.J. Hay, J. Chem. Phys. 66 (1977) 4377.
[25] For some minima, small (up to about $100i$ cm^{-1}) spurious

imaginary frequencies were obtained, corresponding to symmetry-breaking vibrational modes. These frequencies were, however, considered as artifacts due to the noninvariance of the integration grid.

[26] GAUSSIAN94, Revision E.l, M.J. Frisch, G.W. Trucks, H.B. Schlegel, P.M.W. Gill, B.G. Johnson, M.A. Robb, J.R. Cheeseman, T. Keith, G.A. Petersson, J.A. Montgomery, K. Raghavachari, M.A. Al-Laham, V.G. Zakrzewski, J.V. Ortiz, J.B. Foresman, J. Cioslowski, B.B. Stefanov, A. Nanayakkara, M. Challacombe, C.Y. Peng, P.Y. Ayala, W. Chen, M.W. Wong, J.L. Andres, E.S. Replogle, R. Gomperts, R.L. Martin, D.J. Fox, J.S. Binkley, D.J. Defrees, J. Baker, J.P. Stewart, M. Head-Gordon, C. Gonzalez, and J.A. Pople, Gaussian, Inc., Pittsburgh, PA, 1995.

[27] K. Raghavachari, G.W. Trucks, J. Chem. Phys. 91 (1989) 1062.

[28] P.J. Hay, W.R. Wadt, J. Chem. Phys. 82 (1985) 299.

[29] D. Schröder, A. Fiedler, W.A. Herrmann, H. Schwarz, Angew. Chem. Int. Ed. Engl. 34 (1995) 2517.

[30] J.B. Pedley, E.M. Marshall, J. Phys. Chem. Ref. Data 12 (1983) 967.

[31] D.E. Clemmer, J.L. Elkind, N. Aristov, P.B. Armentrout, J. Chem. Phys. 95 (1991) 3387.

[32] R.H. Page, C.S. Gudeman, J. Opt. Soc. Am. B (1990) 1761.

[33] A.D. Sappey, G. Eiden, J.E. Harrington, J.C. Weisshaar, J. Chem. Phys. 90 (1989) 1415.

[34] M.R. Sievers, Y.-M. Chen, P.B. Armentrout, J. Chem. Phys. 105 (1996) 6322.

[35] G. Balducci, G. Gigli, M. Guido, J. Chem. Phys. 79 (1983) 5616.

[36] M.R. Sievers, P.B. Armentrout, Int. J. Mass Spectrom., in press.

[37] M.R. Sievers, P.B. Armentrout J. Chem. Phys. 102 (1995) 754.

[38] U. Mazurek, D. Schröder, H. Schwarz, Coll. Czech. Chem. Comm. 63 (1998) 1498.

[39] C. Shi, M. Xu, M.P. Rosynek, J.H. Lunsford, J. Phys. Chem. 97 (1993) 216.

[40] N.W. Cant, E.M. Kennedy, P.F. Nelson, J. Phys. Chem. 97 (1993) 1445.

[41] C.C.Y. Chow, J.M. Goodings, Can. J. Chem. 73 (1995) 2263.

[42] T.C. Jackson, T.J. Carlin, B.S. Freiser, J. Am. Chem. Soc. 108 (1986) 1120.

[43] P.M.W. Gill, B.G. Johnson, J.A. Pople, Chem. Phys. Lett. 197 (1992) 499.

[44] A.J. Merer, Annu. Rev. Phys. Chem. 40 (1989) 407.

[45] P.E.M. Siegbahn, Chem. Phys. Lett. 201 (1993) 15.

[46] P.E.M. Siegbahn, J. Phys. Chem. 97 (1993) 9096.

[47] P.B. Armentrout, B.L. Kickel, Organometallic Ion Chemistry, B.S. Freiser (Ed.), Kluwer, Dordrecht, 1996, p. 1.

[48] F. Bottomley, L. Sutin, Adv. Organomet. Chem. 28 (1988) 339.

[49] S. Shaik, D. Danovich, A. Fiedler, D. Schröder, H. Schwarz, Helv. Chim. Acta 78 (1995) 1393.

[50] S. Shaik, M. Filatov, D. Schröder, H. Schwarz, Chem. Eur. J. 4 (1998) 193.

[51] For a brief survey and further references, see D. Schröder, H. Schwarz, J. Hrušák, P. Pyykkö, Inorg. Chem. 37 (1998) 624.